Available online at www.sciencedirect.com

jmr&t Journal of Materials Research and Technology

journal homepage: www.elsevier.com/locate/jmrt

Original Article

Thermal expansion behaviour of Invar 36 alloy parts fabricated by wire-arc additive manufacturing

E. Aldalur [a,*], *A. Suárez* [a,b], *F. Veiga* [a,c]

[a] *TECNALIA, Basque Research and Technology Alliance (BRTA), Advanced Manufacturing Department, Paseo Mikeletegi 7, 20009 Donosti, Spain*

[b] *ADDILAN Fabricación Aditiva S.L., Eguzkitza 1, 48200 Durango, Spain*

[c] *Departamento de Ingeniería, Universidad Pública de Navarra (UPNA), Edificio Departamental Los Pinos, Campus Arrosadía, 31006 Iruña, Navarra, Spain*

ARTICLE INFO

Article history:
Received 5 April 2022
Accepted 20 June 2022
Available online 26 June 2022

Keywords:
Additive manufacturing
WAAM
Invar
Dilatometry
GMAW
PAW

ABSTRACT

Invar 36 alloy is of high interest in various industrial sectors, due to its reduced thermal expansion properties. This study aims to validate Wire-Arc Additive Manufacturing (WAAM) technology as a valid method for manufacturing aerospace tooling in Invar 36. The main novelty and the objective of this work is to study the properties of Invar deposited by WAAM technology and to provide guidelines for the manufacture of parts using this technology. To do so, the thermal expansion behaviour of Invar specimens manufactured using Gas Metal Arc Welding (GMAW)-based WAAM technology and Plasma Arc Welding (PAW)-based WAAM technology is analyzed for subsequent comparison with the values obtained from the laminated Invar sample used as the reference specimen. A wall is manufactured with each technology, for comparative purposes, from which specimens were extracted for the dilatometry test and metallographic analysis. The results of these analyses show the advantages of GMAW technology for the manufacture of Invar alloy parts, as it presents the same thermal expansion behaviour as the laminated reference material with less presence of precipitates and no macrostructural failures such as pores, cracks and lacks of fusion. Furthermore, to conclude, an aeronautical tooling that has been manufactured within this work demonstrated the potential of this technology to manufacture specialized aeronautical parts.

* Corresponding author.
E-mail address: eider.aldalur@tecnalia.com (E. Aldalur).

https://doi.org/10.1016/j.jmrt.2022.06.114

1. Introduction

The Invar alloy was discovered by Charles Eduard Guillaume in 1861. This discovery occurred when he was investigating the possibility of an inexpensive material which would vary neither in volume nor in length when exposed to temperature variations [1]. Specifically, his aim was to respond to the need for a material which could maintain the same length at room temperature under different global climatic conditions. Therefore, Invar became a widely used material in precision measurement applications, such as pendulums for clocks, thermostats, and other precision instruments. Nowadays, the applications of Invar alloys are very diverse. They are of great importance in metrology and precision instruments, TV kinescopes, liquid natural gas and cryogenic tanks, orbiting satellites, and aerospace tooling [2,3]. Thus, Invar stands out because of its low Coefficient of Thermal Expansion (CTE), which is due to its relative lack of expansion or contraction with changes in temperature [4]. For this reason, the name Invar was taken from the word invariable [5].

Since its discovery, the Invar alloy has assumed great importance in research. Its unusual physical behaviour of no thermal expansion with temperature change has been observed in Fe–Ni alloys with Ni concentrations within a range of 30–45% [6,7]. The material used in this paper, Invar 36, is within this range with a composition in weight of 64% Fe and 36% Ni. Specifically, this Invar has the lowest CTE value, below 2×10^{-6} K^{-1} [8].

As mentioned, Invar is an alloy, a combination of Ni and Fe. As a metal, Fe has a BCC structure and Ni has an FCC structure. When combined, with an Ni concentration higher than 30%, the alloys are weldable and they have austenitic FCC structures, where Ni is the ϒ stabilizer of iron. In wrought Invar 36, the Curie temperature (Tc) is 279 °C and for applications below this temperature, it shows a very low CTE and ferromagnetic properties [8]. In contrast, above the Tc temperature, the material is already paramagnetic, and the thermal expansion behaviour becomes similar to other materials. Tc peaks at a Ni concentration of approximately 66%. Tc decreases when the Ni concentration drops lower than 40% due to a reduction in permeability [9].

However, alloys with an austenitic structure, such as Invar, are hard to machine because of their high ductility, work hardening and low conductivity [10,11]. Nevertheless, they are adequate for welding [12,13]. Therefore, additive manufacturing is a good alternative to traditional techniques for the manufacture of Invar parts, because these technologies melt the minimum necessary amount of material without extracting the material from a solid block. In the previous literature, the evaluation of the CTE value and Curie temperature in materials processed by additive techniques, mostly, Selective Laser Melting (SLM) and Laser Metal Deposition (LMD), has been exhaustively analyzed. Meanwhile, this issue in Invar deposited using Wire Arc Additive Manufacturing (WAAM) technology has yet to be studied.

On the one hand, Asgari et al. [14] conducted a study in which Fe–Ni (36%) was employed to manufacture samples with SLM technology utilizing different process parameters. These samples were studied with X-ray computed tomography (CT) to look at microstructure, density, structural integrity (determining pore size, morphology and inter-alignment of pores), chemical composition and thermal expansion behaviour. It was concluded that sample densities were higher than 99.8% in all cases and the porosity level decreased at higher laser powers. Furthermore, as is known, the CTE value is highly dependent on the composition of the material. Nevertheless, in this study with the parameters utilized during the SLM process, the chemical composition of the as-built parts was unchanged. As the composition remains unchanged, the influence of density on the CTE was studied. The CTE was shown to decrease alongside a decrease in relative density. However, the CTE values of these samples and the conventionally manufactured Invar alloys were comparable. Furthermore, the direction of additive manufacturing was also observed to affect thermal expansion with some samples built in certain directions yielding higher CTE values.

On the other hand, Yakout et al. [15,16] reported that the CTE value is related to the volumetric energy density of SLM technology. In the SLM process, the volumetric energy density (J/mm^3) is calculated as the ratio between laser power (W) and the multiplication between the average scanning speed (mm/s), hatch spacing (mm) and layer thickness (mm). It was found that there is a critical laser energy density, for which the SLM process is optimal in terms of material properties. This critical energy density achieves stable melting, the homogeneous composition of the melted material, homogeneous microstructure, magnetic properties and CTE values similar to those obtained in the same laminated material. Critical energy of 86.8 J/mm^3 was established for Invar 36 alloy. Below this energy, the manufactured samples showed no significant changes in their composition, but void formation (gas pores or lack of fusion) occurred with a subsequent reduction in the CTE. However, above this critical energy, the number of voids decreased, but the samples showed changes in their composition, reducing the levels of nickel and manganese, and increasing the amount of iron, molybdenum and silicon. This increase in silicon and molybdenum means a reduction in the CTE value and an increase in the magnetic moment of the part [17]. Finally, Wegener et al. manufactured samples using the SLM process with CTE values of 1.8×10^{-6} K^{-1} between 0 and 100 °C that were similar to the values of conventionally processed materials [8].

Furthermore, changing the processing parameters of a LMD process, with a 4 KW CO_2 laser and a four tip coaxial nozzle, yielded CTE values similar to those achieved utilizing conventional processing methods [18]. Finally, as was mentioned above, in the previous literature, few studies have been carried out analyzing the microstructures and the mechanical properties of Invar parts manufactured using WAAM technology and, instead, the thermal expansion behaviour has yet to be studied.

Simplifying, WAAM technology consists of feeding material in wire form and melting it through an electric arc [19]. WAAM process belongs to the Directed Energy Deposition DED technology according to the ISO/ASTM 52900 standard [20]. In this technology parts are manufactured by superimposing layers and it has the capacity for massive material deposition, being able to reach deposition rates of more than 8 kg/h, which is much higher than the typical deposition rate of

powder laser systems (typically up to 1 kg/h). Therefore, although in this process the geometrical resolution is considerably lower than for lasers, WAAM technology is gaining more and more interest in the manufacturing industry, now that this process is one of the most economical methods for manufacturing metallic large parts of medium geometrical complexity. Specifically, the manufacturing of aeronautical tooling with Invar is one of the applications in which WAAM technology could be extremely useful. These tooling techniques are used to manufacture large carbon fiber composite structures for the aeronautical industry. The use of Invar material in these tooling operations is of vital importance since its low CTE means that the composite parts have extremely strict tolerances without losing geometric accuracy, due to the low thermal expansion of the tooling [21–23].

Depending on the nature of the welding source, three types of WAAM processes are distinguished: 1) Gas Metal Arc Welding (GMAW)-based WAAM technology [24], 2) Plasma Arc Welding (PAW)-based WAAM technology [25], 3) Gas Tungsten Arc Welding (GTAW)-based WAAM technology [26], each one with its own characteristics and applications.

In this paper, the thermal expansion shown by Invar specimens manufactured using GMAW-based WAAM technology and PAW-based WAAM technology were analyzed for later comparison with the values of the (reference material) laminated Invar. These two technologies have been chosen within the WAAM processes because these ones offer the greatest advantages and material properties. This study was carried out with the aim of validating the WAAM technology as a reliable method of manufacturing aeronautical tooling from Invar 36 alloys. Therefore, at the end of this work, the manufacture of real tooling using GMAW-based WAAM technology is summarized.

2. Materials and methods

2.1. Materials

A commercial Invar 36 wire with a diameter of 1.2 mm was deposited. The composition of this wire is shown in Table 1. Furthermore, 8 mm thick Invar (UTP A 8036 S) sheets were used as the baseplate.

2.2. Set-up

The samples were manufactured in the Addilan WAAM machine v0.1 (Fig. 1) to carry out the experimentation, which contains its own CNC for additive manufacturing and on-line monitoring and traceability systems. This machine offers the possibility of manufacturing parts using both the GMAW-based WAAM technology and the PAW-based WAAM technology. So, the machine is equipped with the Titan XQ 400 AC puls (EWM) welding source for the GMAW technology and with the Tetrix 552 AC/DC Synergic (EWM) plasma welding source for PAW technology. In this manner, the Addilan machine has interchangeable heads with two torches, one for each technology, as can be seen in Fig. 1. Moreover, a pointer pyrometer (Optris CT) was installed on both heads of the machine (Fig. 1) to measure and to control the temperature of the manufactured samples, which is critical in this type of processes. To set the emissivity of Invar 36 value reported from literature [27] was chosen to be 0.3.

Table 1 – Invar 36 wire composition %wt.

C	Mn	Cr	Ni	Nb	Fe	Ti
0.22	0.43	0.01	35.66	1.38	61.6	0.53

2.3. Manufacturing specifications

In this research, straight walls with each of the above-mentioned technologies and a final validation part were manufactured. First of all, the baseplate was prepared and cleaned to start welding for the manufacture of the walls. Afterwards, the start and end points of welding were entered, thus determining the length of the walls (220 mm). Then, welding began and the beads were added layer by layer.

These walls were manufactured from pairs of overlapping beads and then by superimposing layers on top of the flat baseplate until a wall height of 100 mm was reached. The overlap distance between the beads was 65% of the width of a single bead (6 mm) and during production, alternating layers were provided in opposite directions as can be seen in Fig. 2 to be able to compensate for the geometrical shape.

When manufacturing the overlapped walls, a waiting period between consecutive beads was introduced, so as to avoid excessive thermal input to the parts. In PAW and GMAW-based manufacturing, this period was fixed in 50 s. Furthermore, the temperature of the wall was measured by the pyrometer, during the deposition process and the waiting period. This strategy was employed following the indications of Artaza et al. [28], who call it interpass cooling strategy ICS and aims to stabilize the deposition process to avoid wall collapse, the value of the waiting time has been selected on the basis of previous experimentation [29].

In this work, for the GMAW-based WAAM manufacturing, the pulsed GMAW welding mode was employed, with a torch to substrate inclination of 90° and a 97.5% Ar/2.5% CO_2 shielding gas with a flow rate of 17 L/min. The nozzle diameter was 20 mm with a 15-mm Stick-out. On the other hand, for the PAW-based WAAM manufacturing 100% Ar gas was utilized as the protection and the plasmatic gas, with flow rates of 12 L/min and 1.2 L/min, respectively.

Furthermore, given that this study aims to compare thermal expansion behaviour in the samples manufactured utilizing GMAW-based and PAW-based technologies, the deposition parameters in both cases were chosen to achieve the highest possible deposition rates with same ratios (relation between the Wire Feed Rate (WFR) and Travel Speed (TS)), good penetration, good bead continuity, adequate wetting angle (30°) and similar bead geometry (approximately bead width of 9 mm), but without an excessive thermal input as was explained in more detail in Veiga et al. [29]. Furthermore, a height control system is used in both PAW and GMAW technologies to determine the layer growth. The utilized set of parameters for each technology is summarized in the Table 2 below.

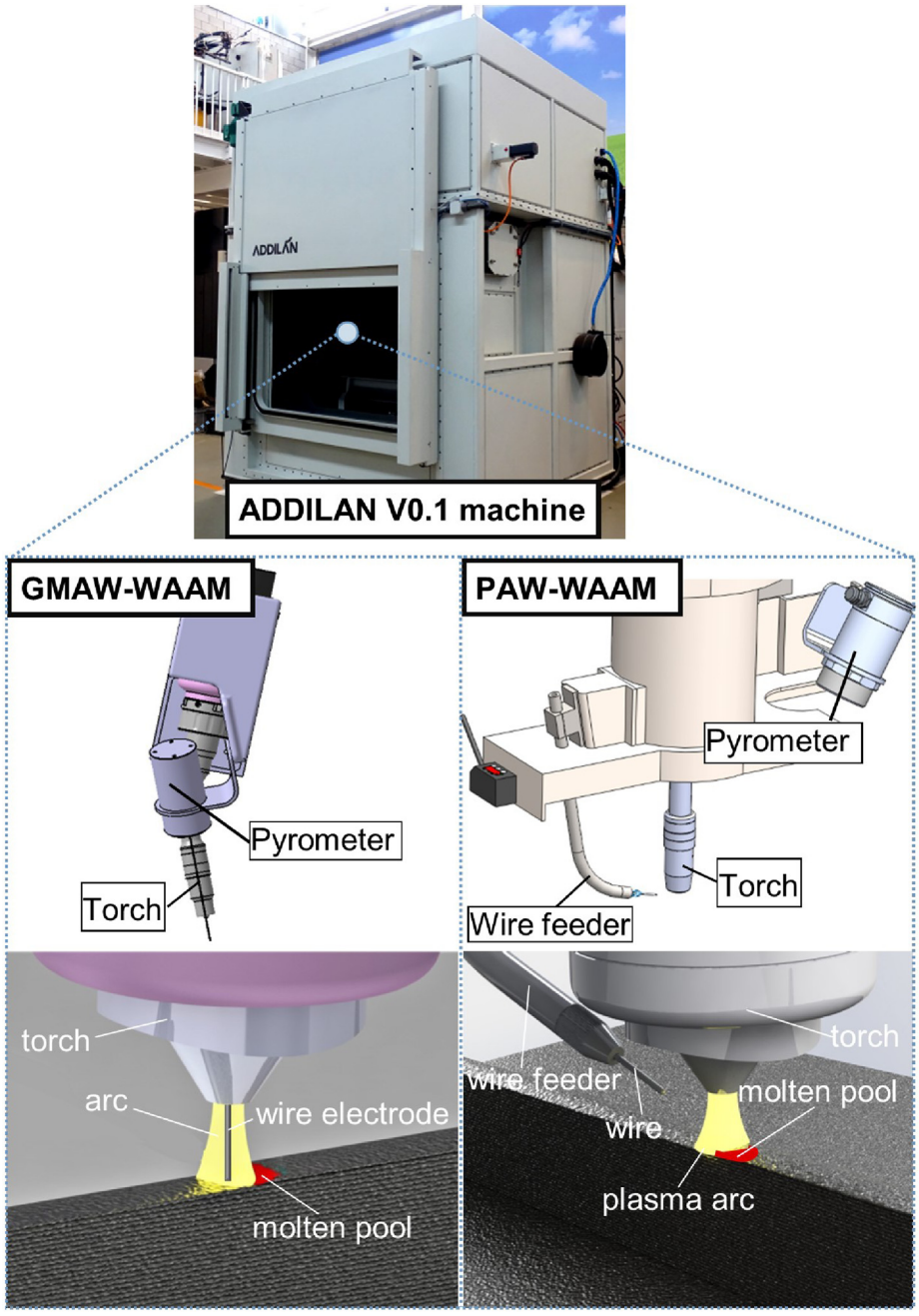

Fig. 1 – Addilan v0.1 WAAM oriented machine with two interchangeable heads: (left) GMAW head and the schematic diagram of GMAW-based WAAM process; (right) PAW head and the schematic diagram of PAW-based WAAM process.

2.4. *Microstructural and thermal characterization*

The walls were transversely cross-sectioned in the middle part and mechanically polished prior to microstructural analysis of the material. These middle parts were observed with a JSM-5910LV (JEOL) Scanning Electron Microscope (SEM) equipped with an EDX Oxford INCA X-act detector and a Tetra (Oxford Instruments) detector. Additionally, regarding the analysis of the microstructure of the fabricated validation part, two samples were machined from the top and low part of its back wall (Fig. 9). Successively, these samples were polished using abrasive grinding papers before etching in Kroll's reagent. After preparing the metallographic samples, the micrographs were recorded with the Eclipse MA200 (Nikon) microscope.

An L78/RITA Quenching Dilatometer from the LINSEIS Thermal Analysis company was used to carry out the dilatometry tests. The samples, with the geometry indicated in Fig. 3a, were machined from the walls. Three samples in the vertical direction and three in the horizontal direction were taken for each wall (manufactured utilizing GMAW-based and PAW-based WAAM technology) for this analysis. Furthermore, three samples were also machined for a commercial laminated Invar 36 sheet (reference material) to compare the

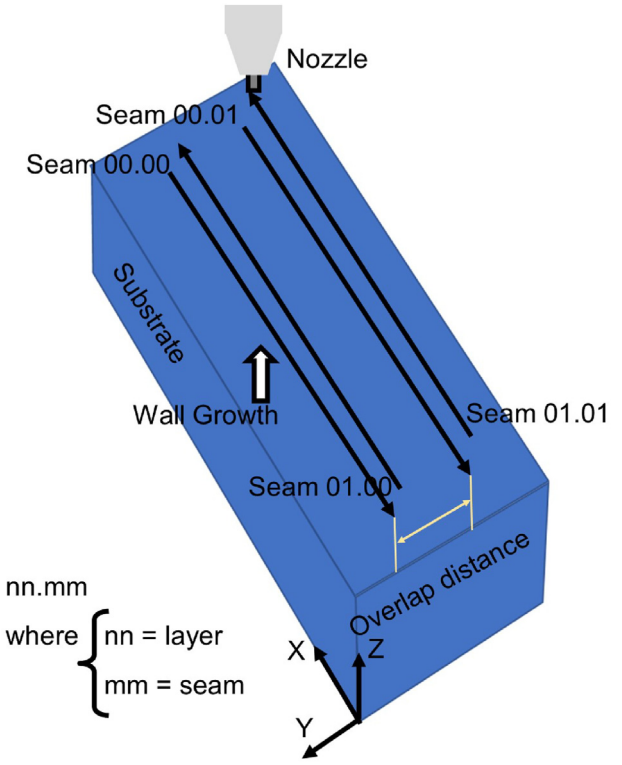

Fig. 2 – Scheme of the deposition process and sequence in WAAM.

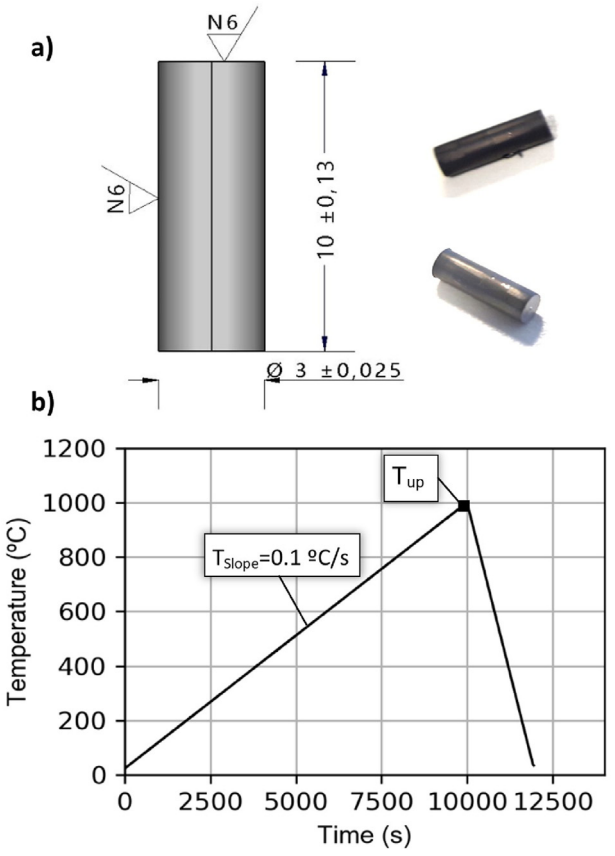

Fig. 3 – a) Geometry of the dilatometry tests samples; b) Heating–Cooling cycle of the study in Invar [16].

results. The dilatometry tests have been carried out according to the ASTM E831-14 standard [30].

The samples were heated in a dilatometer, via an induction copper coil furnace from room temperature to 1000 °C at a heating rate of 0.1 °C/s, each sample taking about 3 h to reach the target temperature. Subsequently, the samples were cooled down to room temperature, within approximately 30 min, as shown in Fig. 3b. The dilatometer is equipped with a Linear Voltage Displacement Transducer (LVDT) to measure the linear deflection (ΔL) utilizing push rods attached to the final part of the sample. Furthermore, a thermocouple is welded to a spot on the sample to measure the temperature during the process.

3. Results and discussion

3.1. *Heat input analysis*

The heat input (HI) parameter or the energy expended on the part during the process is firstly of vital importance for the comparison of the thermal expansion behaviour in the samples manufactured utilizing GMAW-based and PAW-based WAAM technology and the laminated material. The heat input can be calculated as energy introduced per unit length [J/mm] [24] following Eq. (1) or as energy introduced per unit volume [J/mm^3] [31] following Eq. (2).

Table 2 – Manufacturing parameters of overlapped walls.

Technology	WFR [m/min]	TS [cm/min]	Ratio	Waiting time [s]
GMAW	8	80	10	50
PAW	6	60	10	50

$$HI = \frac{\eta * \sum_{i=1}^{n} \frac{I_i * V_i}{n}}{TS} \quad (1)$$

where η is the arc thermal efficiency (in this case 0.9), V_i (V) and I_i (A) are instantaneous voltage and current values and TS is the travel speed. However, if the instantaneous voltage and current values are to be recorded, the voltage and current signals during the manufacture of the walls have also to be acquired. For that reason, the ADDILAN machine has a high-frequency acquisition system installed. The signals once recorded were integrated to introduce in Eq. (1).

Otherwise, Eq. (2) was utilized to calculate heat introduced per unit of volume. In this equation, HI is the energy introduced per unit length calculated in Eq.(1). In this equation, the control area (Δx and Δz) where the heat is introduced was, in this case, the transversal area of each deposited bead. Furthermore, the comparable parameter in the studies on the SLM process, volumetric laser energy density (E_V), was calculated as the ratio between laser power and the multiplication of average scanning speed, hatch space and layer thickness [16].

$$HI_{3D} = \frac{HI}{\Delta x * \Delta z} \quad (2)$$

In Table 3, the main values related to the energy input can be seen. As explained above, both HI and HI_{3D} were calculated using Eq. (1) and Eq. (2).

As can be seen, the energy of the PAW process uses twice the energy of the GMAW process. The PAW process is of very low efficiency process where the plasma arc apart from heating the fed material also heats everything else around it. DuPont et al. [32] reported this effect obtaining an average arc efficiency of 0.47 ± 0.03 in the PAW process, while the efficiency of the GMAW process was 0.84 ± 0.04. This low efficiency is mainly due to dissipation of over half of the radiation and heat by convection from the arc to the nozzle over the tungsten electrode and part of the arc. In these experiments, a metallic nozzle of a certain size was used to act as a heat sink, effectively absorbing energy from the arc before it can be transferred to the material. These heat losses are a significant part of the energy transfer in the PAW process and imply a substantial reduction in arc efficiency in comparison with the GMAW process.

3.2. *Temperature analysis*

As regards the heat input, the temperature gradients during the deposition and the waiting time of a single bead manufactured using each technology can be observed in Fig. 4. These beads were deposited in the middle height of the walls when the process had already stabilized. So, without taking the first layers of the walls into account, because the process had yet to stabilize, the graphs obtained for rest of the deposited beads were similar to those in Fig. 4.

In Fig. 4, the temperature was registered utilizing the pointer pyrometers installed in both machine heads (Fig. 1) that are directed to the heat trails start point, that is, towards the end point of the molten pool. The temperature during the deposition process of the PAW technology was significantly higher, almost double the maximum temperature of the GMAW technology. As explained in section 3.1, it concerns the higher heat input obtained in PAW technology. On the other hand, as can be seen, the cooling curves were similar in both cases, very pronounced at the beginning and more constant at the end. In both cases, although PAW starts from higher temperatures, in order not to increase the manufacturing time greatly, the waiting time was set at 50 s, reaching a temperature of 450 °C in PAW and 310 °C in GMAW.

3.3. *Dilatometry analysis*

A dilatometry analytical test was performed of the wall material, to determine whether WAAM technology can be used to manufacture parts in Invar alloys, such as aeronautical tooling or similar, where the thermal expansion behaviour shown by the material is very important. Three test samples

Table 3 – Main values related to the heat input in both technologies.

Technology	I [A]	V [V]	HI [J/mm]	HI_{3D} [J/mm^3]
PAW	290	34	986	43.59
GMAW	220	27	446	19.72

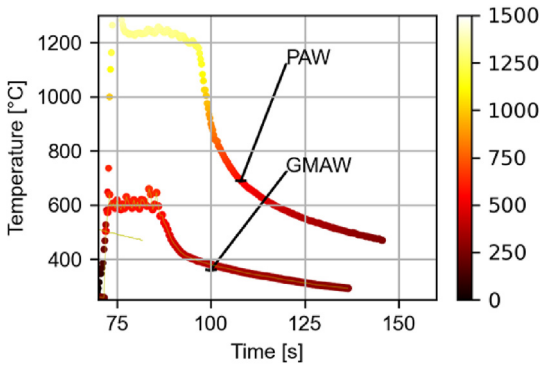

Fig. 4 – Temperature graph during the deposition and the waiting time of a single bead deposited at mid-height of the two walls manufactured utilizing PAW and GMAW-based WAAM technologies.

were taken in the vertical direction and three in the horizontal direction from each of the Invar walls manufactured utilizing the two manufacturing methods (GMAW-based WAAM technology and PAW-based WAAM technology). In addition, this type of test was also performed on three samples machined from commercial laminated Invar 36 material, to use as reference material and for comparison with the final results.

The thermal expansion behaviour of different materials and its measurement can be performed with the dilatometry test. In this type of test, the material is heated and cooled over a controlled cycle (Fig. 3-b) and the linear deflection of the sample is measured. Thus, the CTE [10^{-6} °C^{-1}] is calculated following Eq. (3):

$$CTE = \alpha = \frac{\Delta L}{Lo^{*}\Delta T} \tag{3}$$

where ΔL is the linear deflection, Lo the initial length of the samples and the ΔT the temperature difference for which ΔL is measured. In addition, the Curie temperature (Tc) values were also calculated from the results of the dilatometry test. The Curie temperature is the temperature above which a ferromagnetic material loses its magnetism and low CTE value, behaving like a purely paramagnetic material. In the dilatometry test results, the temperature that corresponds to the point where the tangent deviates from the curve is the Curie temperature.

In this way, the medium heating curves that are the results of the dilatometry tests of the samples machined from the reference material and the walls manufactured utilizing the two WAAM technologies, are shown in Fig. 5. Specifically, in Fig. 5a, the medium heating dilatometry curves, of the reference material and GMAW horizontal and vertical samples can be observed. As can be seen, similar curves were obtained in all the cases and a Curie temperature was established, following the procedure mentioned above, at 332 °C, 340 °C and 365 °C for the reference material, the GMAW horizontal material and the GMAW vertical material, respectively. The difference between the curves of GMAW vertical and horizontal samples was insignificant concluding that the material manufactured through GMAW-based WAAM technology was isotropic regarding its thermal expansion behaviour. In

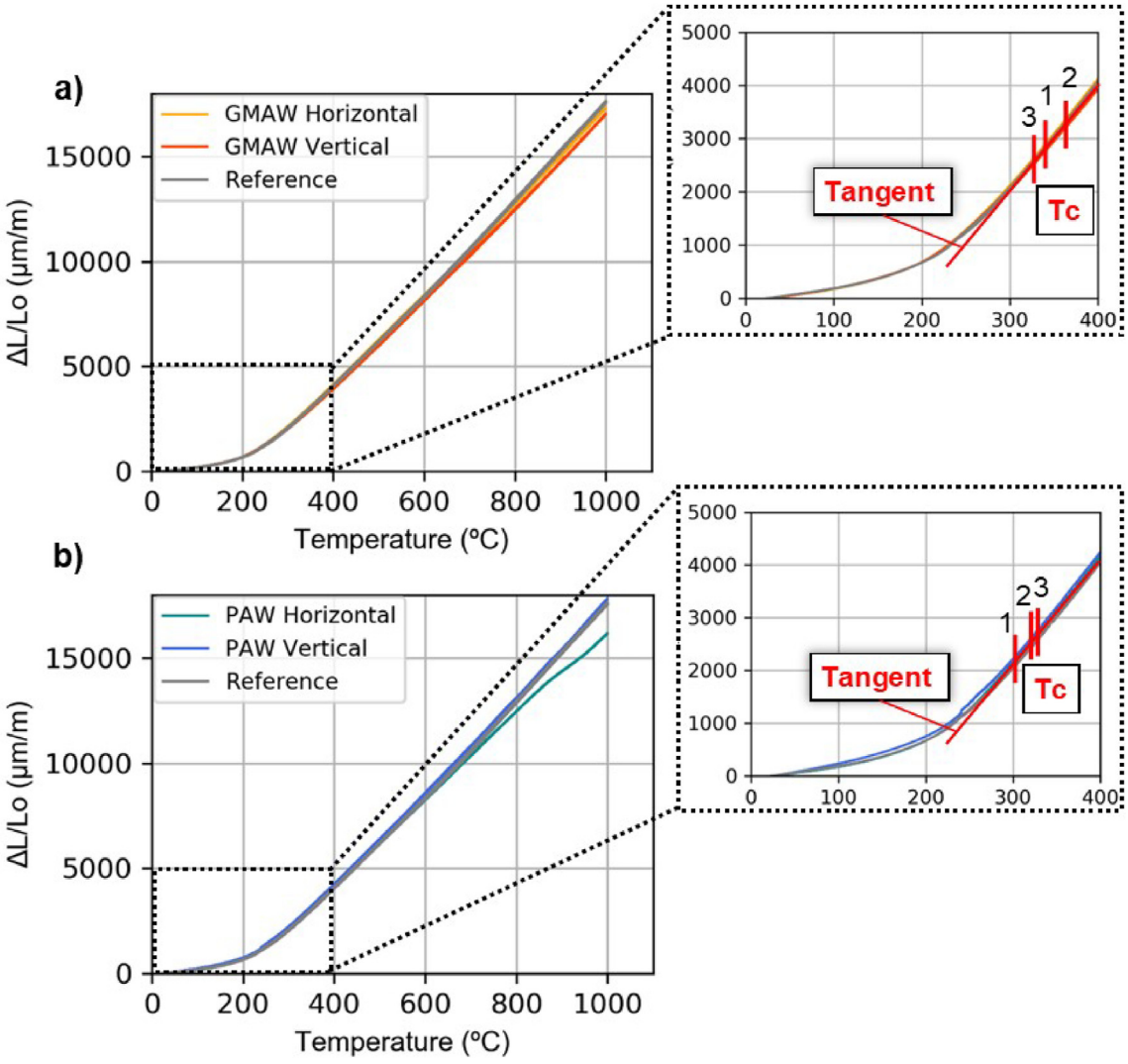

Fig. 5 – Dilatometry curves of the specimens taken from the wall manufactured using a) GMAW-based WAAM technology and the reference material; b) PAW-based WAAM technology and the reference material. Note: in the magnified images the Tc values of each case are marked: 1) horizontal sample; 2) vertical sample; 3) reference sample.

addition, the repeatability of these tests was very high in the three specimens manufactured in each case.

Moreover, the medium dilatometry curves, heating curves, of the reference material and PAW horizontal and vertical samples are shown in Fig. 5b. The Curie temperature was established at 302 °C and 327 °C for PAW horizontal and PAW vertical, respectively, as can be seen in the mini-enlargement of the graph in Fig. 5b. The reference material Curie temperature, as mentioned, was above 332 °C. As can be seen, regarding the Curie temperature, some dissimilarities found between horizontal and vertical directions in the GMAW and the PAW technologies were always higher in the vertical direction. Furthermore, the material manufactured utilizing GMAW technology showed higher Curie temperatures than the material manufactured using PAW technology. These small differences observed in the coefficient of expansion observed in both directions are due to the anisotropic nature of the material manufactured by WAAM, as the grain is elongated in the direction of wall growth, as has been addressed in previous papers [29] and reviews of the subject [33].

Regarding the calculated CTE values following Eq. (3), in Fig. 6, the evolution of this value with respect to temperature can be observed. As can be seen, similar curves were obtained in the reference material and in the samples manufactured by GMAW-based WAAM technology, concluding that the thermal expansion behaviour of the material manufactured by GMAW was practically equal to the reference material. This shows that the Invar tooling manufactured by GMAW-based WAAM had a similar CTE to the laminated material, concluding that this novel technology can be used to manufacture parts from Invar alloy with adequate thermal behaviour.

These results also agreed with a conclusion obtained by other authors relating to SLM technology. In SLM technology a critical laser energy density introduced per unit volume exists, for which the SLM process is optimal in terms of material properties. This critical laser energy was determined at 86.8 J/mm^3 for the Invar 36 alloy [15–17]. With this critical energy

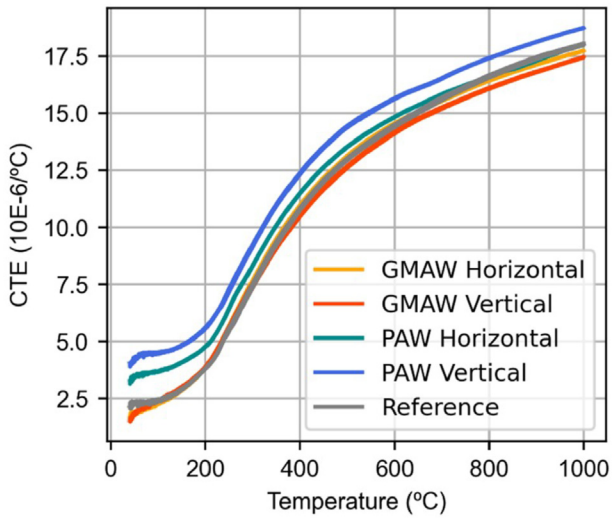

Fig. 6 – CTE value evolution with respect to the temperature.

density, the CTE values were similar to those obtained in the same laminated material. Above this critical energy level, the samples showed changes in their composition, reducing the levels of nickel and manganese, and increasing the amount of iron, molybdenum and silicon. This increase in silicon and molybdenum implied a reduction in the CTE values.

Nevertheless, with the GMAW-based WAAM process, the heat inputs per unit of volume were lower, never achieving the critical energy of 86.8 J/mm^3. As was calculated in section 3.1, a heat input of 19.72 J/mm^3 was obtained in the case of GMAW-based WAAM technology. For this reason and agreeing with the conclusion on SLM technology, the CTE values and the dilatometry curves of the materials manufactured using GMAW-based WAAM technology and the reference material of laminated Invar were highly similar. Furthermore, the critical energy density void formation was observed in the SLM process below, with a subsequent reduction in the CTE value, due to the powder nature of the fed material. This problem is not presented in GMAW-based WAAM technology, because no pores of melting lacks are observed in the material, as is shown in the following section.

On the other hand, in the case of PAW technology, the CTE evolution curves are somewhat different in the initial part, that is, for low temperatures. For more details, the average CTE values for temperatures up to 100 °C and their standard deviation can be seen in Table 4 for all the samples. It is clear that in the case of GMAW technology, an isotropic material is obtained with CTE values similar to those obtained in the laminated reference test material. In addition, these values were also in agreement with the those reported in the previous literature. For example, Wegener et al. [8] obtained CTE values of 1.8 $\times$ 10^{-6} K^{-1} between 0 and 100 °C in samples manufactured with the SLM process. Likewise, Yang et al. [34] obtained CTE values lower than 2.0 $\times$ 10^{-6} K^{-1} (standard value of laminated Invar 36 [35]) in their samples manufactured with different laser energy density levels. Otherwise, in the samples manufactured by means of PAW technology, the CTE average values were higher within low temperature ranges

Table 4 – Average CTE values and its standard deviation for all types of samples.

Sample	Average CTE 0–100 °C [10^{-6} C^{-1}]	Σ
GMAW Horizontal	1.94	0.095
GMAW Vertical	1.96	0.18
PAW Horizontal	3.5	0.1
PAW Vertical	4.32	0.16
Reference	2.29	0.05

than the values of the reference material, even when the energy of this process was 43.59 J/mm^3 (calculated in section 3.1) lower than the critical energy of 86.8 J/mm^3 determined by various authors as the critical energy for the SLM process [15]. So, in the next section, the microstructure obtained in these samples will be studied, in order to determine the cause of this phenomenon.

To sum up, the material manufactured by GMAW-based WAAM had the same thermal expansion behaviour and the same CTE value as the laminated reference material. It was therefore concluded that GMAW-based WAAM technology can be used for the manufacturing of Invar 36 parts. since the material that is obtained maintains the behaviour of reduced thermal expansion, so characteristic and suitable for the various applications in which the Invar 36 alloy is present. The samples manufactured using the PAW-based WAAM technology showed higher CTE values than the reference material, so an attempt to determine the cause is also described in the following section.

3.4. *SEM analysis*

SEM analysis was performed to observe the microstructure of the Invar walls made by GMAW and PAW-based WAAM technologies. Since the material manufactured using GMAW technology and the reference material presented similar thermal expansion behaviours, but the material manufactured using the PAW process presented a slightly different thermal expansion behaviour, it was verified whether the different heat input of each process had affected their microstructure.

On the one hand, as can be seen in Fig. 7, dendritic structures were obtained in both cases. In the material manufactured using GMAW, this structure was more homogeneous with well-defined cellular dendritic constructions (Fig. 7–1). Furthermore, in the limits of the dendrites, niobium segregations were found, marked in a lighter color in the micrograph. As can be clearly seen in the SEM-EDX patterns of point A, corresponding to the limit of these dendrites, the composition in weight has high percentages of niobium. The composition of this area in weight was exactly 14.19% C, 4.3% Ti, 36.26% Fe, 21.45% Ni and 23.79% Nb. Therefore, it was concluded that niobium carbons were present at the limit of the dendrites. Nevertheless, at point B, corresponding to a zone that is not at the limit of the dendrites, a composition in weight was similar to the composition of the fed wire, 2.2% C, 0.62% Ti, 59.63% Fe, 35.08% Ni and 2.45% Nb.

On the other hand, a dendritic structure is also shown in Fig. 7–2 that represents the microstructure of the wall

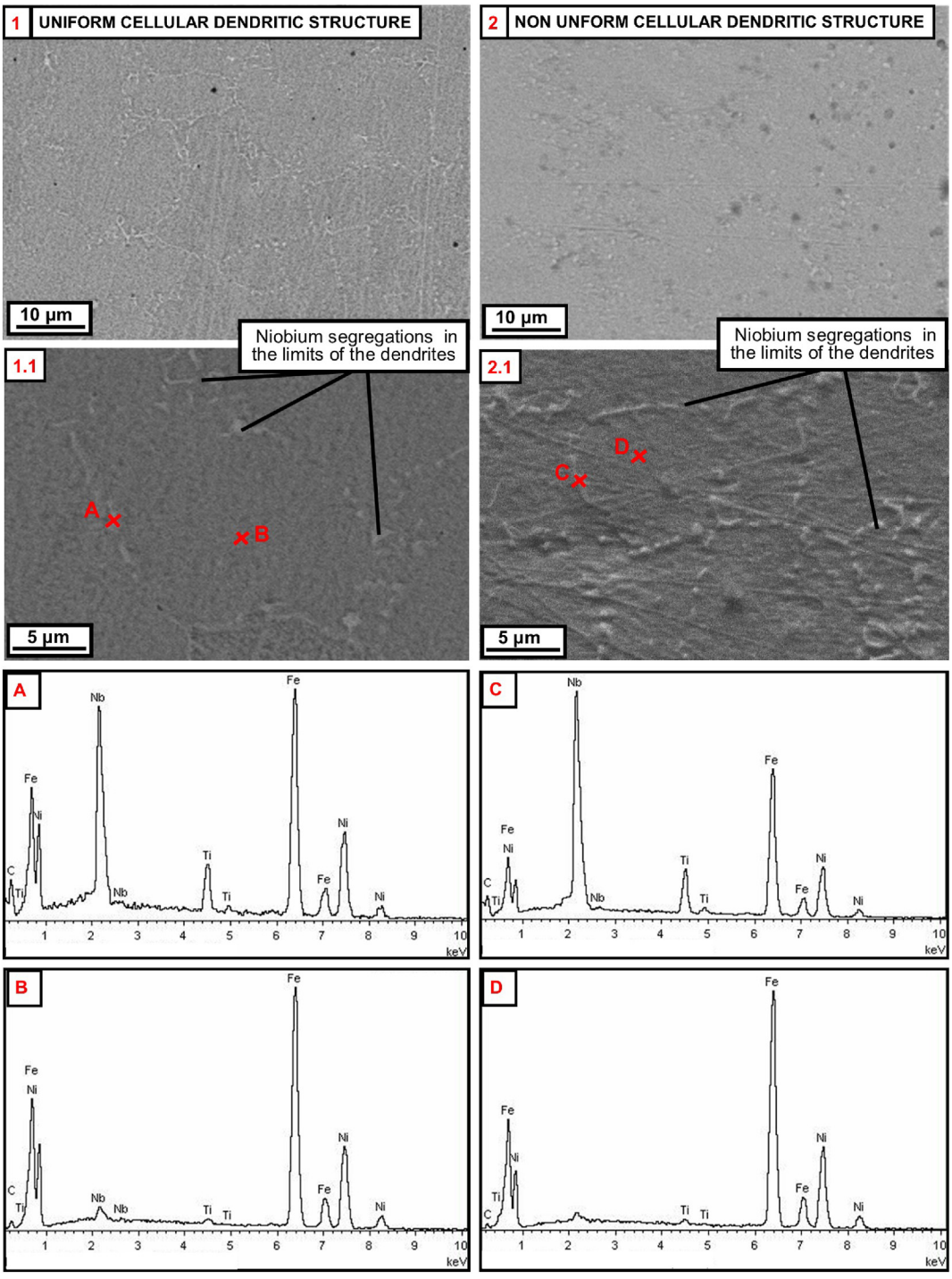

Fig. 7 – SEM micrographs 1) of the samples taken from the wall manufactured utilizing GMAW-based WAAM process indicating a magnification in 1.1 and the SEM-EDX patterns at points A and B; 2) of the samples taken from the wall manufactured utilizing PAW-based WAAM process indicating the magnification in 2.1 and the SEM-EDX patterns at points C and D.

manufactured utilizing PAW-based WAAM technology. In this case, unlike what happened with the GMAW manufactured material, this structure was not uniform and well-defined. In the limits of the dendrites, niobium segregations were also found, marked in a lighter color in the micrograph, as is evident from the composition represented in the SEM-EDX patterns at point C. The composition in weight at point C was 12.98% C, 5.3% Ti, 31.75% Fe, 16.49% Ni and 33.49% Nb, with high percentages of Nb. However, at point D, which was not within the limit of the dendrites, a composition in weight of 4.77% C, 0.61% Ti, 60.96% Fe and 33.67% Ni was obtained, similar to the composition of the wire fed process.

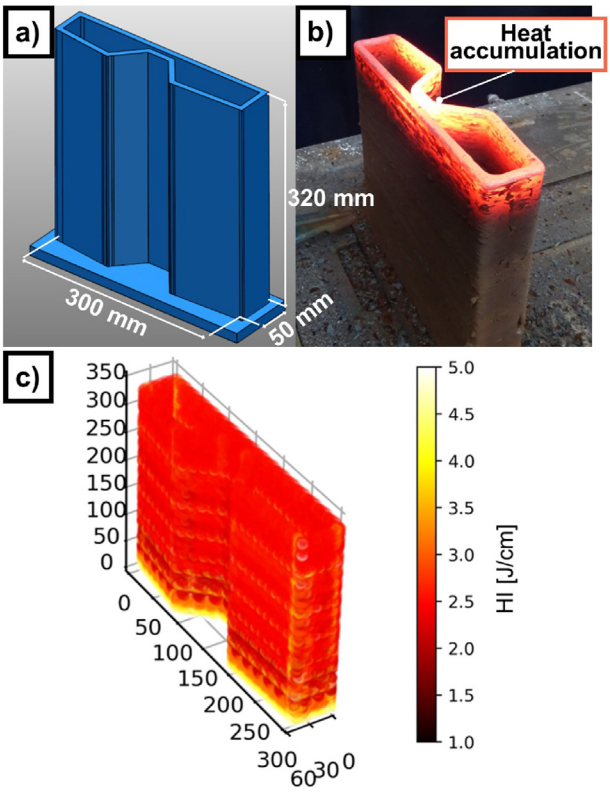

Fig. 8 – a) Tooling design; b) fabrication process for the tooling; c) heat input (HI) representation in tooling manufacturing.

In this way, it was concluded that materials with no macrostructural failures such as pores, cracks or lack of fusion were manufactured using both technologies. Moreover, in both cases, dendritic structures were obtained with niobium carbides at the extreme ends of these dendrites. In previous studies, it was found that susceptibility to solidification cracking decreased with carbon and niobium additions to Invar 36 alloy [36]. Specifically, in the solidification process, this addition reduced the temperature range where both solid and liquid exist together as a result of the decreasing niobium quantity in the residual liquid, due to the formation of niobium carbides. An effect that decreased susceptibility to solidification cracking. To do so, the addition of niobium has to be in a range of less than 1.5% in weight, in Invar alloys containing 0.2% carbon [36], as is the case of the material under study. Consequently, in this type of Invar, as demonstrated in this study, niobium carbides were produced in the dendrite space of primary austenite [37].

In conclusion, the only difference between the materials manufactured using the two WAAM technologies was that, in the case of GMAW-based WAAM technology, the material has more homogeneous and well-defined dendrites, which means that the presence of precipitates is lower than in PAW samples as can be seen in Fig. 7–1.1 and 1.2. This difference in the quantity and the organization of the carbides was due to the different heat input and consequently, different temperatures reached in the material during the deposition process, obtaining lower temperatures in the GMAW process which creates a less abrupt cooling and therefore, fewer carbides.

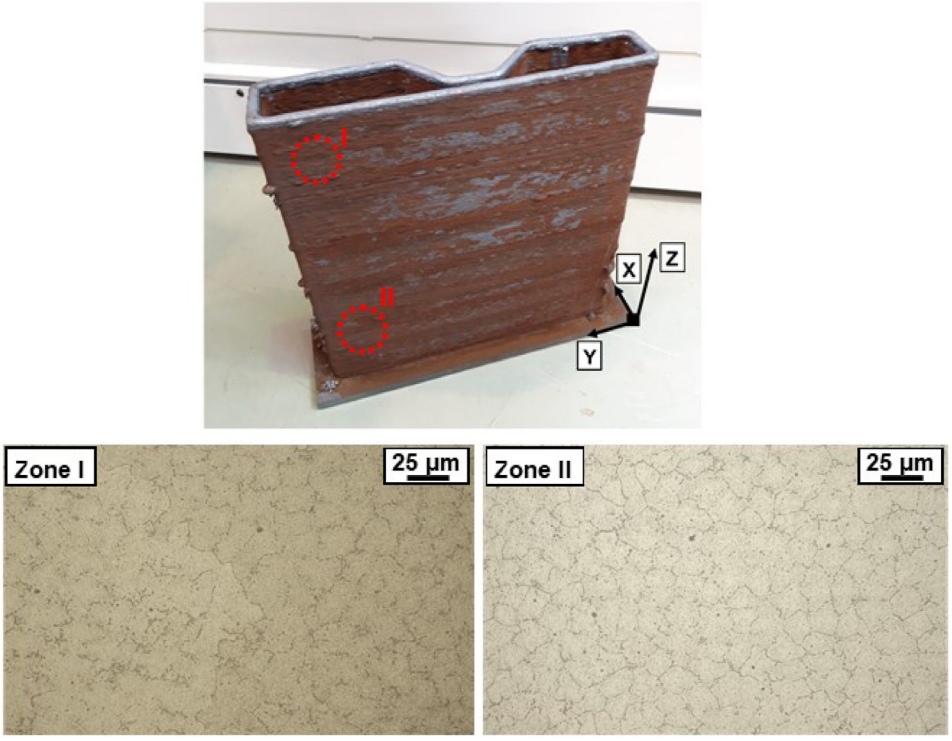

Fig. 9 – Material extraction areas (zone I and zone II) to observe the microstructure in the use case and microstructure in the YZ plane of zone I and zone II.

3.5. *Use case*

Once it had been demonstrated that the material manufactured by GMAW-based WAAM was in terms of thermal expansion behaving in the same way as the reference laminated material, then a use case was proposed, to illustrate that WAAM technology can be used for the manufacturing of real parts in Invar 36. This use case was an aeronautical tooling (Fig. 8a, size 300 x 320 × 50 mm) where the characteristics of thermal expansion of the material are vital.

WAAM-based GMAW technology was selected for the manufacture of this use case, because the thermal expansion properties achieved with this technology are more adequate and of greater similarity to the reference material. This similarity of thermal expansion was because GMAW achieved a more homogeneous microstructure with less presence of precipitates and no macrostructural failures such as pores, cracks or lack of fusion. Furthermore, the arc efficiency of the GMAW process was higher than the PAW process and the energy introduced in the process to melt the same amount of material was lower. In this way, the part was not exposed to excessive heat, given the lower heat input of the GMAW process.

Taking into account the design of the part, the material was deposited continuously in a single bead. The parameters and the fabrication conditions were the same as those of the wall manufactured using GMAW-based WAAM technology. The only difference is that as the tooling was overheated (Fig. 8b), the travel speed was increased until 160 cm/min after the first layers. This variation in the travel speed can be shown in the representation of the energy introduced per unit length, in Fig. 8c, where higher energy was introduced in the first layers than in the others.

After the use case manufacturing, two samples were extracted from the top and low zones of its back wall, areas marked in red in Fig. 9, to observe whether there was any change in the microstructure of the manufactured part, due to the thermal effects of the process in comparison with the wall. As can be seen in Fig. 9, no differences are seen between the microstructure of zones I and II. In addition, the microstructure was very similar to the previously manufactured wall utilizing GMAW-based WAAM technology that was characterized as having a wall microstructure with a dendritic structure.

4. Conclusions

In this paper, both thermal and microstructural characterizations of Invar 36 alloy manufactured utilizing two types of (PAW-based and GMAW-based) WAAM technology are presented for the purpose of validating the WAAM technology as a reliable method for tooling aeronautical parts in this material. Some of the conclusions reached from this study are as follows:

- In PAW technology, the heat input was two times greater than that of the GMAW process which was due to the very low arc efficiency of the PAW process. Furthermore, because of that, the temperature during the PAW deposition process was almost double than in the case of GMAW technology.
- From the dilatometry results, similar curves were obtained in the reference laminated material and in the material manufactured using GMAW-based WAAM technology. This shows that the Invar manufactured by GMAW has an analogous CTE to the laminated material, concluding that this novel technology can be used to manufacture Invar into parts with adequate thermal behaviour. In contrast, the samples manufactured using the PAW-based WAAM technology showed CTE values higher than the reference material.
- The Curie temperature was set at 332 °C, 340 °C, 365 °C, 302 °C and 327 °C for the reference material, for horizontal GMAW, vertical GMAW, horizontal PAW and vertical PAW, respectively. Some dissimilarity was found between the Curie temperatures in the horizontal and the vertical directions. Furthermore, the material manufactured utilizing GMAW technology showed higher Curie temperatures than the material manufactured using PAW technology.
- No macrostructural failures such as pores, cracks or lack of fusion were found in the SEM analysis of the microstructure, in the material manufactured utilizing GMAW and PAW processes. Furthermore, in both cases, similar dendritic formations were observed at the ends of which niobium carbides were found. A higher concentration of niobium carbides was found in the Invar material produced by PAW than in the sample produced by GMAW. In this last case, the material had more homogeneous and well-defined dendrites, due to the lower heat input of the deposition process.
- Finally, taking into account the results obtained from the analysis of the two WAAM technologies, efficient tooling of Invar 36 with GMAW-based WAAM technology has been performed in an adequate manner, without variation or errors in its microstructure.

Funding

The authors acknowledge the Basque Government for financing the ADDHOC project, HAZITEK 2021 program (ZL-2021/00989) and EKOHEGAZ ELKARTEK program (kk-2021/00092).

Declaration of Competing Interest

The authors declare that they have no known competing financial interests or personal relationships that could have appeared to influence the work reported in this paper.

REFERENCES

[1] Gillaume CE. Invar and its applications. Nature 1904;71:134–9.
[2] Liu H, Sun Z, Wang G, Sun X, Li J, Xue F, et al. Effect of aging on microstructures and properties of Mo-alloyed Fe-36Ni invar alloy. Mater Sci Eng, A 2016;654:107–12. https://doi.org/10.1016/j.msea.2015.12.018.

[3] Chen C, Ma B, Liu B, He J, Xue H, Zuo Y, et al. Refinement mechanism and physical properties of arc melted invar alloy with different modifiers. Mater Chem Phys 2019;227:138–47. https://doi.org/10.1016/j.matchemphys.2019.02.006.
[4] Abbasi SM, Morakabati M, Mahdavi R, Momeni A. Effect of microalloying additions on the hot ductility of cast FeNi36. J Alloys Compd 2015;639:602–10. https://doi.org/10.1016/j.jallcom.2015.03.167.
[5] Davis JR. Alloying: understanding the basics. 2001.
[6] Ananthanarayanan NI, Peavler RJ. A new reversible solid-state trans- formation in iron-nickel alloys in the lnvar range of compositions. Nature 1961;192:962–3.
[7] Acharya SS, Medicherla VRR, Bapna K, Ali K, Biswas D, Rawat R, et al. Mixed ground state in Fe-Ni Invar alloys. J Alloys Compd 2021;863:158605. https://doi.org/10.1016/j.jallcom.2021.158605.
[8] Wegener T, Brenne F, Fischer A, Möller T, Hauck C, Auernhammer S, et al. On the structural integrity of Fe-36Ni Invar alloy processed by selective laser melting. Addit Manuf 2021;37. https://doi.org/10.1016/j.addma.2020.101603.
[9] Sahoo A, Medicherla VRR. Fe-Ni Invar alloys: a review. Mater Today Proc 2020;43:2242–4. https://doi.org/10.1016/j.matpr.2020.12.527.
[10] Kim SH, Choi SG, Choi WK, Yang BY, Lee ES. Pulse electrochemical machining on Invar alloy: optical microscopic/SEM and non-contact 3D measurement study of surface analyses. Appl Surf Sci 2014;314:822–31. https://doi.org/10.1016/j.apsusc.2014.07.028.
[11] Kim SH, Choi SG, Choi WK, Lee ES. Surface characteristics of invar alloy according to micro-pulse electrochemical machining. Mater Technol 2017;51:745–9. https://doi.org/10.17222/mit.2016.187.
[12] Zhao Y, Wu AP, Ren JL, Sato YS, Kokawa H, Miyake M, et al. Temperature and force response characteristics of friction stir welding on invar 36 alloy. Sci Technol Weld Join 2013;18:232–8. https://doi.org/10.1179/1362171812Y.0000000077.
[13] Jiang Z, Chen X, Li H, Lei Z, Chen Y, Wu S, et al. Grain refinement and laser energy distribution during laser oscillating welding of Invar alloy. Mater Des 2020;186:108195. https://doi.org/10.1016/j.matdes.2019.108195.
[14] Asgari H, Salarian M, Ma H, Olubamiji A, Vlasea M. On thermal expansion behavior of invar alloy fabricated by modulated laser powder bed fusion. Mater Des 2018;160:895–905. https://doi.org/10.1016/j.matdes.2018.10.025.
[15] Yakout M, Elbestawi MA. Insights on laser additive manufacturing of invar 36. 2020. p. 71–93. https://doi.org/10.4018/978-1-7998-4054-1.ch004.
[16] Yakout M, Elbestawi MA, Veldhuis SC. A study of thermal expansion coefficients and microstructure during selective laser melting of Invar 36 and stainless steel 316L. Addit Manuf 2018;24:405–18. https://doi.org/10.1016/j.addma.2018.09.035.
[17] Garibaldi M, Ashcroft I, Simonelli M, Hague R. Metallurgy of high-silicon steel parts produced using Selective Laser Melting. Acta Mater 2016;110:207–16. https://doi.org/10.1016/j.actamat.2016.03.037.
[18] Tan H, Wang Y, Wang G, Zhang F, Fan W, Feng Z, et al. Investigation on microstructure and properties of laser solid formed low expansion Invar 36 alloy. J Mater Res Technol 2020;9:5827–39. https://doi.org/10.1016/j.jmrt.2020.03.108.
[19] Williams SW, Martina F, Addison AC, Ding J, Pardal G, Colegrove P. Wire + Arc additive manufacturing. Mater Sci Technol 2016;32:641–7. https://doi.org/10.1179/1743284715Y.0000000073.
[20] ISO/ASTM, ISO/ASTM 52900: additive manufacturing. General principles. Terminology; 2015.
[21] Yan L. Wire and Arc Additive manufacture (WAAM) reusable tooling investigation. 2013.
[22] Chu JB. Investigating the feasibility and impact of integrating Wire-Arc additive manufacturing in aerospace tooling applications by. 2020.
[23] Williams S. Use of WAAM for manufacture of reconfigurable tooling with conformal features. WAAMMat 2015.
[24] Aldalur E, Suárez A, Veiga F. Metal transfer modes for Wire Arc Additive Manufacturing Al-Mg alloys: influence of heat input in microstructure and porosity. J Mater Process Technol 2021;297. https://doi.org/10.1016/j.jmatprotec.2021.117271.
[25] Artaza T, Suárez A, Veiga F, Braceras I, Tabernero I, Larrañaga O, et al. Wire arc additive manufacturing Ti6Al4V aeronautical parts using plasma arc welding: analysis of heat-treatment processes in different atmospheres. J Mater Res Technol 2020;9:15454–66. https://doi.org/10.1016/j.jmrt.2020.11.012.
[26] Qi Z, Cong B, Qi B, Sun H, Zhao G, Ding J. Microstructure and mechanical properties of double-wire + arc additively manufactured Al-Cu-Mg alloys. J Mater Process Technol 2018;255:347–53. https://doi.org/10.1016/j.jmatprotec.2017.12.019.
[27] Yakout M, Phillips I, Elbestawi MA, Fang Q. In-situ monitoring and detection of spatter agglomeration and delamination during laser-based powder bed fusion of Invar 36. Opt Laser Technol 2021;136:106741. https://doi.org/10.1016/j.optlastec.2020.106741.
[28] Artaza T, Bhujangrao T, Suárez A, Veiga F, Lamikiz A. Influence of heat input on the formation of laves phases and hot cracking in plasma arc welding (PAW) additive manufacturing of inconel 718. Metals 2020;10:771. https://doi.org/10.3390/met10060771.
[29] Veiga F, Súarez A, Artaza T, Aldalur E. Effect of the heat input on wire-arc additive manufacturing of Invar 36 alloy: microstructure and mechanical properties. Weld World 2022;66:1081–91. https://doi.org/10.1007/s40194-022-01295-4.
[30] Astm E831-14. Standard test method for linear thermal expansion of solid materials by thermomechanical analysis. West Conshohocken: ASTM International; 2014 [PA].
[31] Aldalur E, Veiga F, Suárez A, Bilbao J, Lamikiz A. High deposition wire arc additive manufacturing of mild steel: strategies and heat input effect on microstructure and mechanical properties. J Manuf Process 2020;58:615–26. https://doi.org/10.1016/j.jmapro.2020.08.060.
[32] DuPont JN, Marder AR. Thermal efficiency of arc welding processes. Weld J 1995;74:406 [s].
[33] Yakout M, Elbestawi MA, Veldhuis SC. A review of metal additive manufacturing technologies. Solid State Phenom 2018;278:1–14. https://doi.org/10.4028/www.scientific.net/ssp.278.1.
[34] Yang Q, Wei K, Yang X, Xie H, Qu Z, Fang D. Microstructures and unique low thermal expansion of Invar 36 alloy fabricated by selective laser melting. Mater Char 2020;166:110409. https://doi.org/10.1016/j.matchar.2020.110409.
[35] Callister WD. Materials science and engineering: an introduction. 7th ed. NY: John Wiley & Sons; 2010.
[36] Hirata H, Ogawa K, Hongou S, Kumagai T, Yamakawa T, Koga S, et al. Effects of carbon and niobium on solidification cracking in Fe-36%Ni invar alloy. Welding of Fe-36%Ni invar alloy. Q J Jpn Weld Soc 2001;19:680–7.
[37] Xu PQ, Zhao XJ, Xu Lnl GX, Sy Z. Microstructure characterisation and CTE study of Fe—42Ni—Nb invar alloys. Mater Sci Technol 2011;27.